International Journal of Minerals, Metallurgy and Materials
Volume 24, Number 3, March 2017, Page 229
DOI: 10.1007/s12613-017-1400-y

Kinetics of thermal decomposition of hydrated minerals associated with hematite ore in a fluidized bed reactor

P.C. Beuria[1)], *S.K. Biswal*[1)], *B.K. Mishra*[1)], *and G.G. Roy*[2)]

1) Institute of Minerals and Materials Technology, Council of Scientific & Industrial Research, Bhubaneswar-751013, India

2) Indian Institute of Technology, Kharagpur-721302, India

(Received: 26 April 2016; revised: 19 October 2016; accepted: 20 October 2016)

Abstract: The kinetics of removal of loss on ignition (LOI) by thermal decomposition of hydrated minerals present in natural iron ores (i.e., kaolinite, gibbsite, and goethite) was investigated in a laboratory-scale vertical fluidized bed reactor (FBR) using isothermal methods of kinetic analysis. Experiments in the FBR in batch processes were carried out at different temperatures (300 to 1200°C) and residence time (1 to 30 min) for four different iron ore samples with various LOIs (2.34wt% to 9.83wt%). The operating velocity was maintained in the range from 1.2 to 1.4 times the minimum fluidization velocity (U_{mf}). We observed that, below a certain critical temperature, the FBR did not effectively reduce the LOI to a desired level even with increased residence time. The results of this study indicate that the LOI level could be reduced by 90% within 1 min of residence time at 1100°C. The kinetics for low-LOI samples (<6wt%) indicates two different reaction mechanisms in two temperature regimes. At lower temperatures (300 to 700°C), the kinetics is characterized by a lower activation energy (diffusion-controlled physical moisture removal), followed by a higher activation energy (chemically controlled removal of LOI). In the case of high-LOI samples, three different kinetics mechanisms prevail at different temperature regimes. At temperature up to 450°C, diffusion kinetics prevails (removal of physical moisture); at temperature from 450 to 650°C, chemical kinetics dominates during removal of matrix moisture. At temperatures greater than 650°C, nucleation and growth begins to influence the rate of removal of LOI.

Keywords: thermal decomposition; fluidized beds; kinetic analysis; hydrated iron ore; activation energy

1. Introduction

Indian iron ore resources are mostly hematite based. Approximately 2×10^{10} t of hematite ore resources are available in India [1]. Day by day, the high-quality iron ore in mines is being depleted, whereas the demand for iron ore increases. At present, India is producing approximately 90 million tons per annum (MTPA) of steel and is planning to produce 3×10^{8} t of steel annually by 2025 [2]. As a result, the demand for iron ore will increase exponentially. It is the need of the hour to utilize the low grade iron ore by adopting suitable process to maximize the recovery of the iron values. The up-gradation of iron ore mostly depends on its mineralogical, physical, and chemical characteristics.

In general, hematite ore in India is associated with goethite, kaolinite gibbsite, and quartzite mineral phases. Goethite and limonite are generated through weathering of hematite. Goethite has been observed to associate either with the parent material hematite or clay minerals. The goethite associated with hematite is called vitreous goethite, whereas that associated with clay minerals is called ochreous goethite [1]. Vitreous goethite is more fragile than ochreous goethite. During either beneficiation or preparation of pellet feed materials, ultra-fine particles are generated. As a result, the Blaine number of pellet feed materials is increased because of the high specific surface area of the fine particles.

Pelletization is considered one of the best options for utilizing iron ore fine concentrate. Pellets are preferred because their excellent physical and metallurgical properties enable their use in blast furnaces or in direct-reduced iron (DRI) processes. Technologies (straight grate or grate kiln) are available for utilizing hematite iron ore concentrate with a low loss on ignition (LOI < 2.5%) and a specific Blaine

Corresponding author: P.C. Beuria E-mail: pcbeuria@immt.res.in

number (1800–2000 cm^2/g). However, iron ore with an LOI greater than 3% adversely affects the quality and productivity of the pellets [3–5]. In present commercial practice, the process parameters are adjusted in the induration process to achieve the optimal quality of pellets by sacrificing plant productivity.

One option for improving the productivity of pelletization plants is to reduce the matrix moisture of the iron ore concentrate via the oxidation roasting process. Gibbsite and goethite release their matrix water molecules within the temperature range from 300 to 400°C, whereas kaolinite releases its matrix moisture at approximately 850°C [2–3]. The heating cycle in the oxidation roasting process is an important parameter in optimizing the reduction of LOI in the iron ore. During oxidation roasting under either static or dynamic conditions, goethite changes to hematite after releasing water [6]. The kinetics of LOI under dynamic conditions is much faster than that under static conditions because dynamic conditions provide greater heat and mass transfer. Hence, we used a fluidized bed roasting system in this study to effectively remove matrix moisture from iron ore fines. This system is needed for analyzing the macro-level effect of the process and design parameters on the kinetics of the solid-state reaction. In the present work, we systematically investigate the effect of temperature and residence time on four iron ore samples with different LOIs.

In the present study, we designed a novel gas–solid batch fluidized bed reactor (FBR) to study the kinetics and mechanism of thermal decomposition of hydrated minerals such as goethite, kaolinite, and gibbsite associated with hematite. The FBR has several advantages: (1) it enables pulse feeding and rapid heating of the particles; (2) it enables utilization of fine iron ores; and (3) it leads to minimization of intraparticle diffusion. Furthermore, it enables the measurement of temperature across the fluidized bed for optimal energy use. In this paper, the most common methods for isothermal kinetic analysis are used to determine the mechanism of decomposition of hydrated minerals present in low-grade iron ore using a fluidized bed furnace and a thermogravimetric analyzer and to evaluate the activation energy. The thermal decomposition of goethite and kaolinite is given in equations (1) and (2), respectively:

$$2FeOOH = Fe_2O_3 + H_2O \quad (1)$$

$$Al_2Si_2O_5(OH)_4 = Al_2O_3 + 2SiO_2 + 2H_2O \quad (2)$$

2. Fluidized bed reactor design

A schematic of the batch FBR is shown in Fig. 1(a). The fluidized bed column with a diameter of 0.1 m and a height of 1.8 m is made of Inconel 625 alloy steel and can withstand temperatures up to 1250°C. It comprises an air compressor, an air by pass valve, a refrigerator dryer, pressure valves, a rotameter bank, an air distributor, and a fluidization column equipped with an electrical heater and thermocouples for measuring temperature. The fluidized bed column has a plenum chamber at its bottom; this chamber is connected to the air inlet pipe. A metallic air distributor (wire mesh) with a pore size of 150 μm is fitted at the bottom of the fluidized bed column, and the top portion of the plenum chamber is filled with 16-mm steel balls supported by 2 mm wire mesh. The steel balls in the plenum chamber ensure that a uniform flow of air enters the fluidizing chamber across the cross section. The fluidizing chamber is

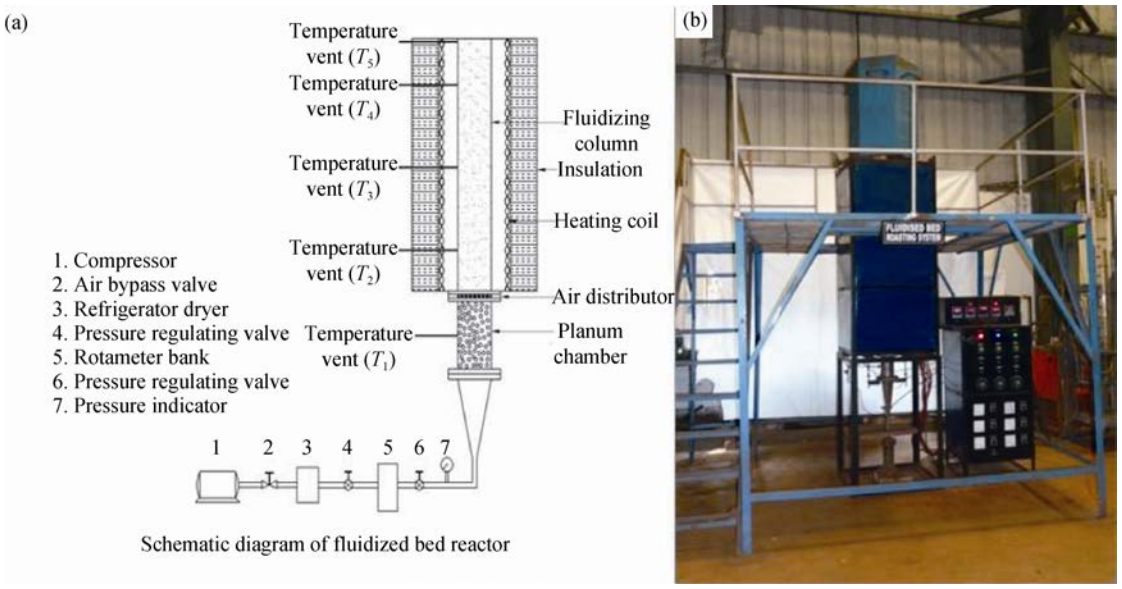

Fig. 1. (a) Schematic and (b) photograph of the fluidized bed reactor used in the experiments.

heated using an electrical heating arrangement with three different heating zones (0.5 m each). The FBR can be maintained at temperatures as high as 1200°C with fluctuations of ±10°C and is accurately controlled using proportional integral derivative (PID) controllers. Thermocouples are inserted into the fluidized bed chamber at different points in the fluidized system, starting at the plenum chambers and continuing to the exit point. The temperature of each point is displayed digitally on the control panel. A photograph of the complete setup is shown in Fig. 1(b).

3. Materials and methods

Four iron ore samples designated as A, B, C, and D with different chemical compositions and LOIs were used in the experiments. Samples A and D are natural iron ore samples collected from the Barbil region of Odisha, India, whereas samples B and C are synthetic mixtures of samples A and D blended in different ratios. The LOIs of samples A, B, C, and D are 2.34wt%, 4.81wt%, 7.36wt%, and 9.83wt%, respectively. The temperature of the FBR was maintained by three PID controllers. A heating rate of 10–15°C/min was used with a minimal supply of air (40 L/min) to avoid any damage to the fluidized bed column because of overheating. After the system attained the specified temperature, the air flow was instantaneously shut off and the 1-kg sample was fed in pulse into the FBR. Air was then allowed into the reactor at a constant flow rate of 100 L/min with an operating velocity ranging from 1.2 to 1.4 times the minimum fluidization velocity (U_{mf}) of the iron ore particles to ensure complete fluidization [7]. After a fixed residence time, the air flow was shut off for a while and a small amount of representative sample was scooped from the bed of particles for measurement of the LOI at that particular temperature and residence time. The percentage of removal of LOI corresponding to the particular residence time and temperature was calculated. The same procedure was followed for different temperatures (from 300 to 1200°C at 50°C intervals) and residence time (1, 2, 3, 4, 5, 10, 15, 20, 25, and 30 min). A fresh sample was collected for each experiment. The same experimental procedures were followed for all of the other investigated iron ore samples. The mineralogical characteristics of the samples after LOI were studied by XRD.

4. Results and discussion

4.1. Characterization of the samples

The mineralogical characteristics of samples were characterized using an X-ray diffractometer (PANalytical X'pert, The Netherlands). Quantitative analysis was carried out via the Rietveld method using the High Score Plus software. The mineralogical characteristics of the samples are presented in Table 1. Sample A contains more hematite, whereas sample D contains more goethite. Similarly, sample A contains less kaolinite and sample D contains more kaolinite. Hence, sample D exhibits a greater LOI than sample A. The concentrations of major and minor compounds such as Fe_2O_3, SiO_2, and Al_2O_3 were quantitatively analyzed by wet chemical analysis using standard methods. For the analysis of trace compounds (K_2O, MgO, MnO_2, P_2O_5, TiO_2, and Na_2O), an inductively coupled plasma optical emission spectroscopy (ICP–OES) (Model No.: optima 8300; Make: Perkin-Elmer) was used. The LOI was analyzed using the standard thermal procedure. The detailed chemical analysis results for the samples are given in Table 2. The Fe content in sample A is greater than that in sample D. The silica and alumina contents of sample D are greater than those of sample A. The particle size analysis was carried out using standard ASTM sieves. The mass distribution of different size fractions is given in Table 3. Compared to sample A, sample D contains a larger fraction of particles smaller than 45 μm. The characteristics of samples B and C fall within those for samples A and D.

Table 1. Mineralogical constituents of the ore samples

wt%

Ore sample	Hematite	Goethite	Kaolinite	Quartzite
Sample A	75.81	15.85	5.29	1.69
Sample B	51.85	38.27	6.76	1.64
Sample C	27.10	61.36	8.27	1.59
Sample D	3.11	83.78	9.74	1.55

Table 2. Chemical analysis results for the ore samples wt%

Ore sample	Fe	Al_2O_3	SiO_2	CaO	K_2O	MgO	MnO_2	P_2O_5	TiO_2	Na_2O	LOI
Sample A	62.98	2.09	4.15	0.080	0.030	0.000	0.150	0.000	0.050	0.040	2.34
Sample B	60.30	2.67	4.79	0.063	0.050	0.000	1.104	0.000	0.035	0.059	4.81
Sample C	57.55	3.27	5.44	0.050	0.070	0.010	1.970	0.000	0.023	0.080	7.36
Sample D	54.87	3.85	6.08	0.030	0.120	0.080	3.430	0.000	0.014	0.100	9.83

Table 3. Size analysis results for the ore samples

wt%

Size / μm	Sample A	Sample B	Sample C	Sample D
+100	6.07	5.10	4.12	3.17
–100+75	9.34	7.33	5.23	3.23
–75+45	18.25	16.24	14.18	12.20
–45	66.34	71.33	76.47	80.86

4.2. Simultaneous differential thermal analysis (SDTA) and thermogravimetric analysis (TGA)

SDTA was carried out to determine the range of temperatures at which the matrix moisture was released from the ore in the small-mass system. The SDTA/TGA curves for samples A, B, C, and D are shown in Figs. 2(a)–2(d), respectively. This figure shows that the removal of LOI starts at 250°C in all the samples. Between 350 and 500°C, the samples lose approximately 80% to 90% of LOI because the major source of moisture in the samples is goethite, which normally releases matrix moisture at 350–400°C. We also observed another ΔT peak at approximately 900°C, indicating final removal of LOI by kaolinite decomposition, especially for samples C and D.

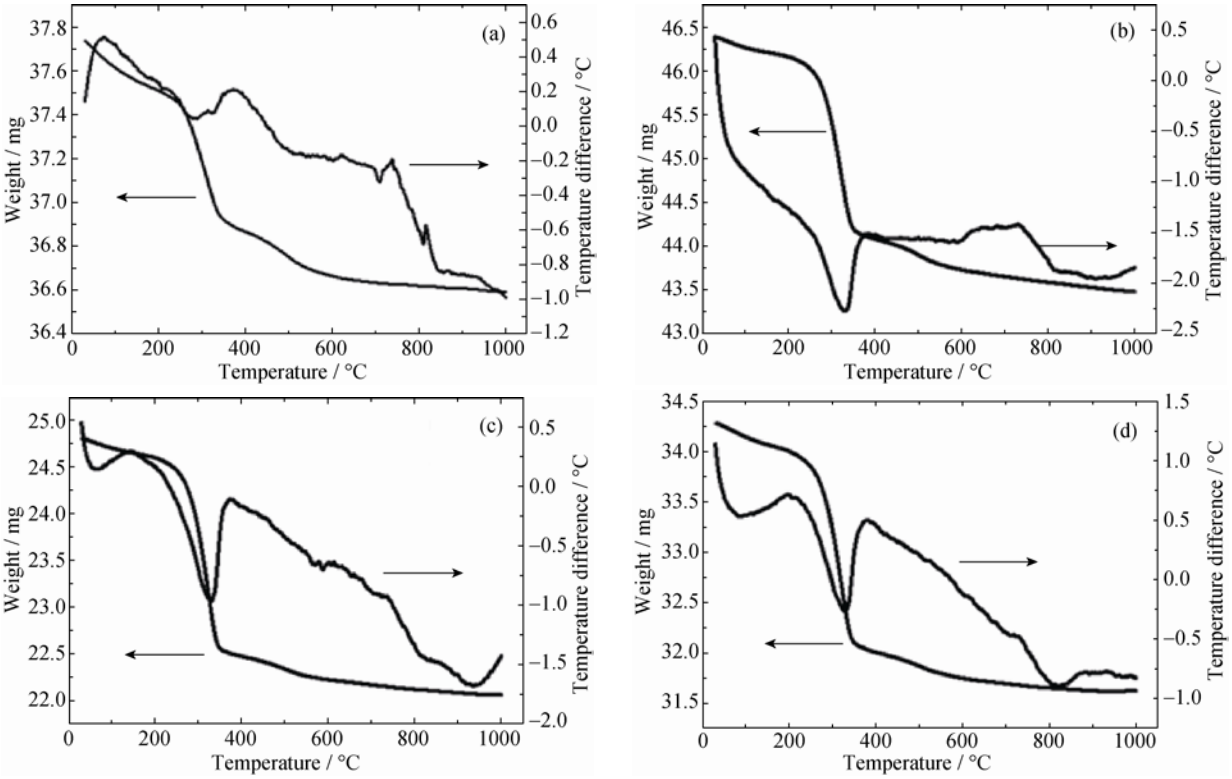

Fig. 2. TGA results for the ore samples: (a) sample A; (b) sample B; (c) sample C; and (d) sample D.

4.3. Effect of temperature and residence time

The variation of removal of LOI with temperature for all samples at different residence time of 1, 5, 15, and 30 min are shown in Figs. 3(a), 3(b), 3(c), and 3(d), respectively. We observed that LOI removal follows S-shaped curve for samples C and D with relatively high LOIs (7.36wt% and 9.83wt%, respectively). By contrast, in the case of low-LOI samples A and B, most of the LOI removal occurs at 300°C and the kinetics become insensitive to temperature at higher temperatures. In the case of high-LOI samples D and C, the LOI removal at 400°C is only 10% and 30%, respectively. By contrast, for samples A and B with lower LOIs, significant amounts (60%–80%) of LOI were removed at 400°C. In the case of sample D, the LOI removal rate becomes high and temperature sensitive beyond 500°C. This sample loses most of its LOI by 700°C; beyond 700°C, the removal rate again becomes less sensitive to temperature. Similar effects were observed at all residence time. These results therefore clearly indicate that three distinct kinetics mechanisms prevail for high-LOI samples over the investigated temperature regimes; by contrast, two mechanisms would explain the LOI removal from low-LOI samples. We further note that the total LOI cannot be removed at 800°C because kaolinite requires a temperature greater than 850°C to release water molecules from its matrix. Thus, a temperature greater than 850°C is required to ensure complete removal of the LOI contributed by kaolinite.

The variation of LOI removal as a function of residence time at different temperatures for samples A, B, C, and D are shown in Figs. 4(a), 4(b), 4(c), and 4(d), respectively. Notably, most of the LOI was removed within 5 min; longer

residence time did not substantially influence the LOI removal. By contrast, temperature dictates the maximum level of LOI removal from the sample. These figures also clearly demonstrate that temperature influences the LOI removal more strongly in the case of high-LOI samples than in the case of low-LOI samples.

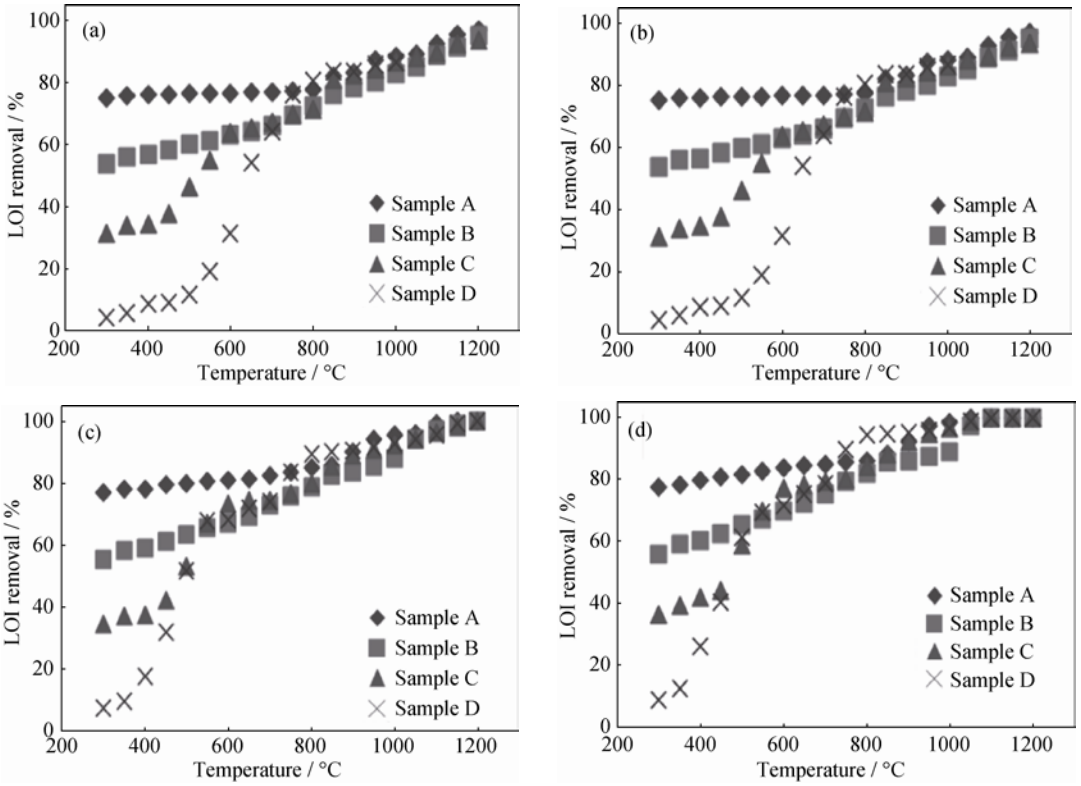

Fig. 3. Variation of LOI removal with temperature at different residence time: (a) 1 min; (b) 5 min; (c) 15 min; (d) 30 min.

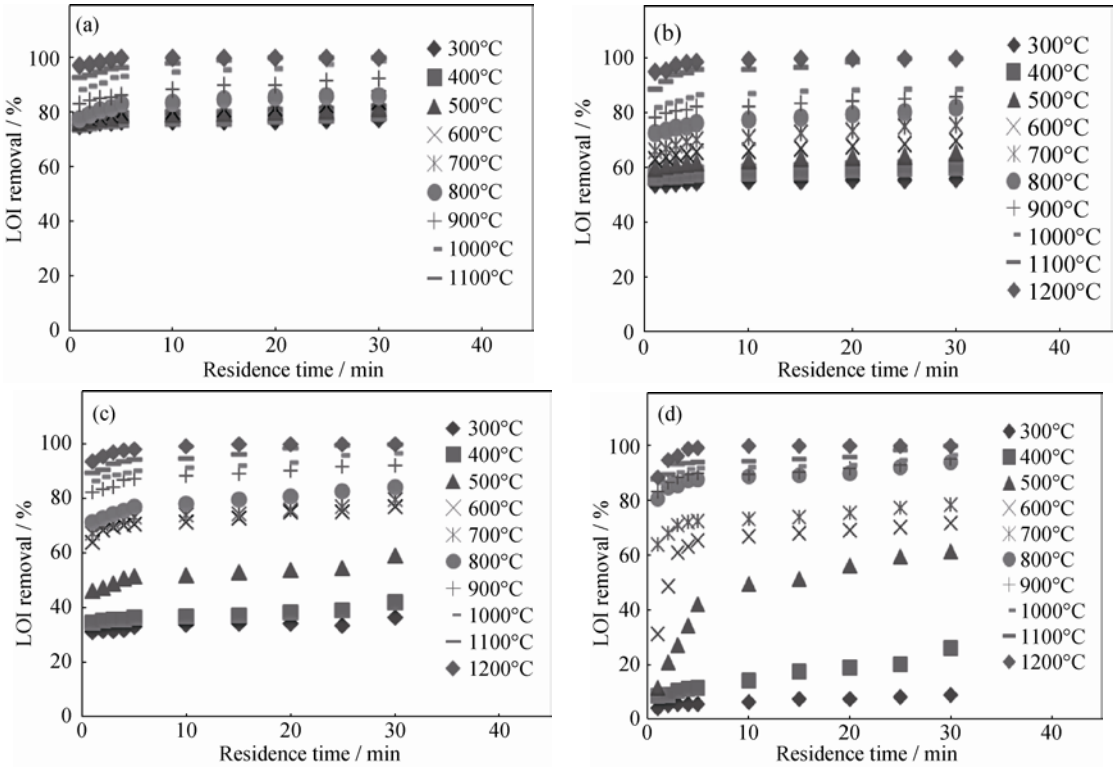

Fig. 4. Variation of LOI removal with residence time at different temperatures for samples A (a), B (b), C (c), and D (d).

4.4. Mineralogy at different temperatures

Quantitative mineralogy by XRD (Rietveld analysis) was carried out on the bulk samples and after thermal decomposition at 400, 700, and 1100°C. The XRD analysis results for raw and roasted sample A at 400, 700, and 1100°C after 1 min of residence time are shown in Fig. 5(a), 5(b), 5(c), and 5(d), respectively. Fig. 6 shows the similar figure for sample D. As per the mineralogical analysis, the major minerals in the bulk sample are hematite, goethite, kaolinite, and quartzite and the concentrations of goethite and kaolinite are

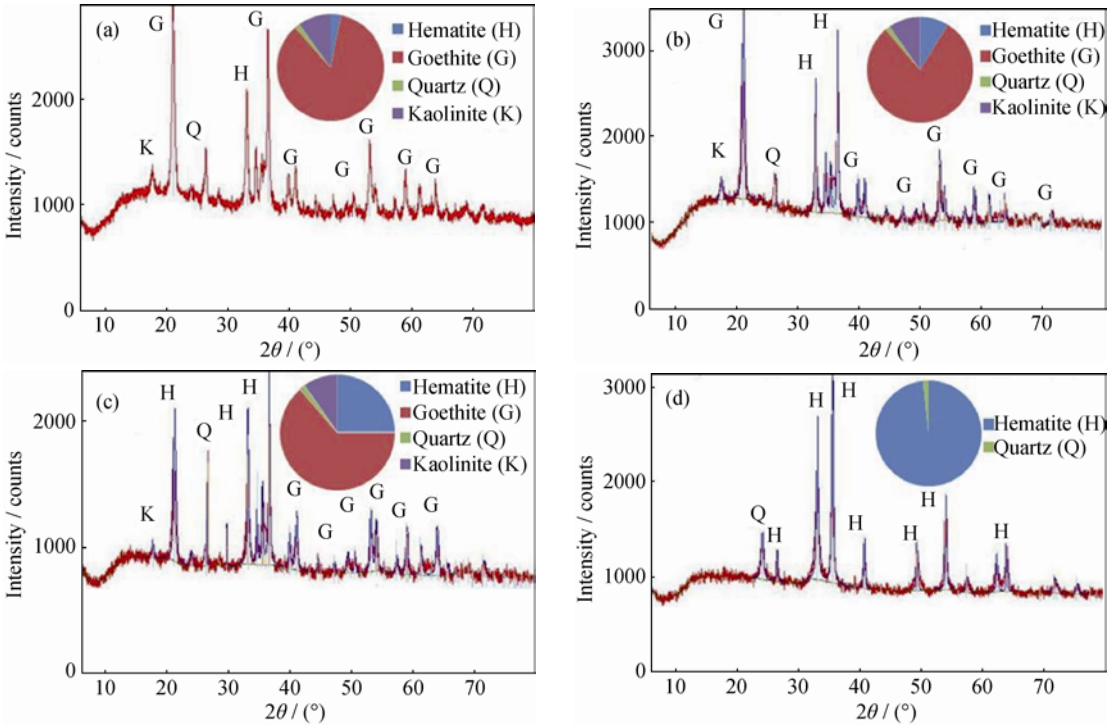

Fig. 5. XRD patterns of sample A: (a) feed material; (b) roasted at 400°C for 1 min; (c) roasted at 700°C for 1 min; (d) roasted at 1100°C for 1 min.

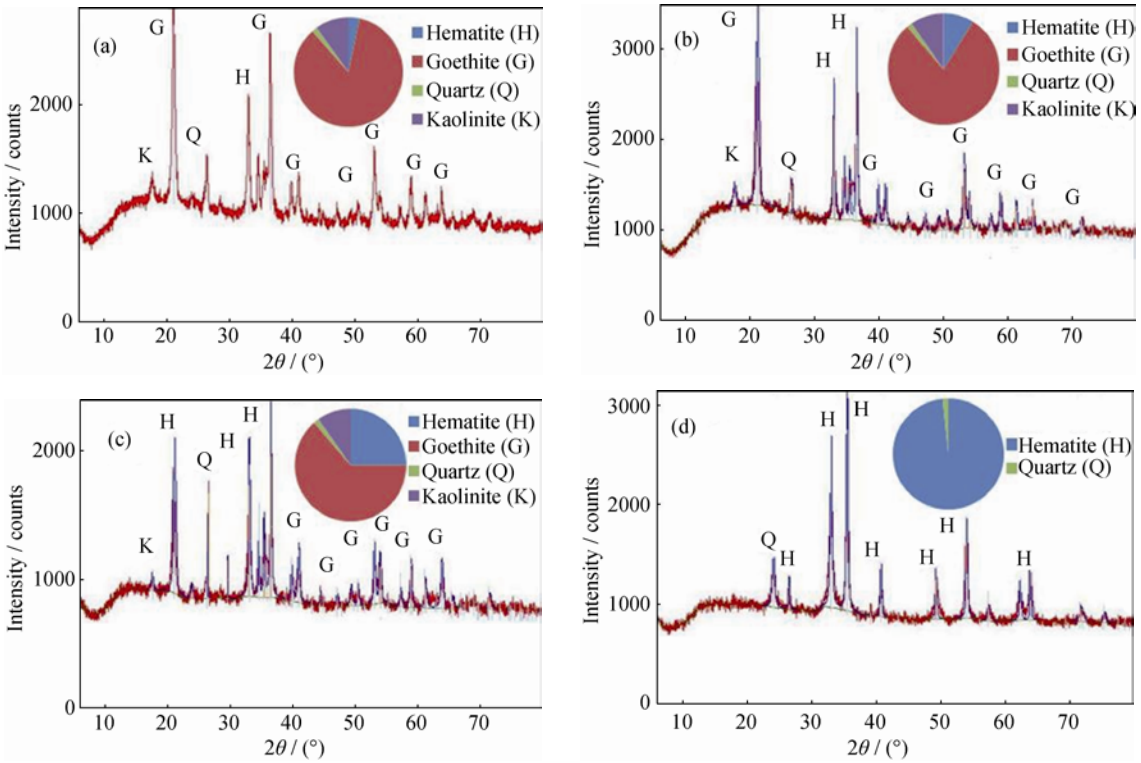

Fig. 6. XRD patterns for sample D: (a) feed material; (b) roasted at 400°C for 1 min; (c) roasted at 700°C for 1 min; (d) roasted at 1100°C for 1 min.

higher in the high-LOI samples. When comparing the XRD patterns of the roasted samples, we observed that, on increasing roasting temperature for all of the samples, the peaks of hydrated minerals (goethite and kaolinite) decreased in intensity and their share in the pie-chart gradually vanished, whereas the peaks of hematite increased in intensity [8]. The majority of LOI contributed by goethite was removed by 700°C, as verified by the absence of goethite in the XRD pattern of sample A roasted at 700°C (Fig. 5). The goethite peaks in the pattern of sample D also became minimal after the sample was roasted at 700°C. We observed that, for sample D, which exhibits a significant LOI associated with kaolinite, 100% removal of LOI requires a temperature greater than 850°C, where kaolinite releases its matrix moisture. This observation is evidenced in Fig. 6 (pie-chart), where the phase change between 700 and 1100°C is substantial, in contrast to Fig. 5 for sample A. A major fraction of kaolinite present in the samples became amorphous after liberation of its matrix moisture and was therefore not visible in the XRD patterns of samples heated beyond 900°C [9].

4.5. Kinetics analysis

A need exists for a detailed investigation of the kinetics of LOI removal as a function of various operational parameters, viz. residence time and temperature under fluidization conditions.

The kinetics of all solid-state reactions can be represented by the general equation:

$$g(\alpha) = kt \tag{3}$$

where α is the fractional conversion (fraction of LOI removed) in time t, and the function $g(\alpha)$ depends on the thermal decomposition mechanism of the iron ore, on the temperature and pressure, and on the physical properties of the particles, i.e., grain size, shape, and crystallinity. The rate of a solid-state reaction can be described by

$$\frac{\mathrm{d}\alpha}{\mathrm{d}t} = \mathrm{A}\mathrm{e}^{-\frac{E_\mathrm{a}}{RT}} f(\alpha) \tag{4}$$

where A is the pre-exponential (frequency) factor, E_a is the activation energy, T is the absolute temperature, R is the gas constant, and $f(\alpha)$ is the inverse of the first derivative of $g(\alpha)$ with respect to α. The rate-determining step in any solid-phase reaction can be evaluated either by diffusion or by a chemical reaction process [10–11]. In these two fundamental processes, surface diffusion results in rapid coating of the surface of the reacting particle with a continuous product layer. Another approach is to consider nucleation of the product's active sites [12–13]. Accordingly, the kinetic function $g(\alpha)$ is represented by three general models: diffusion, chemical reaction, and nucleation [14–16].

A typical graphical representation of the rate of thermal decomposition with time ($\mathrm{d}\alpha/\mathrm{d}t$ vs. t) at different temperatures for samples A, B, C, and D is shown in Figs. 7(a)–7(d),

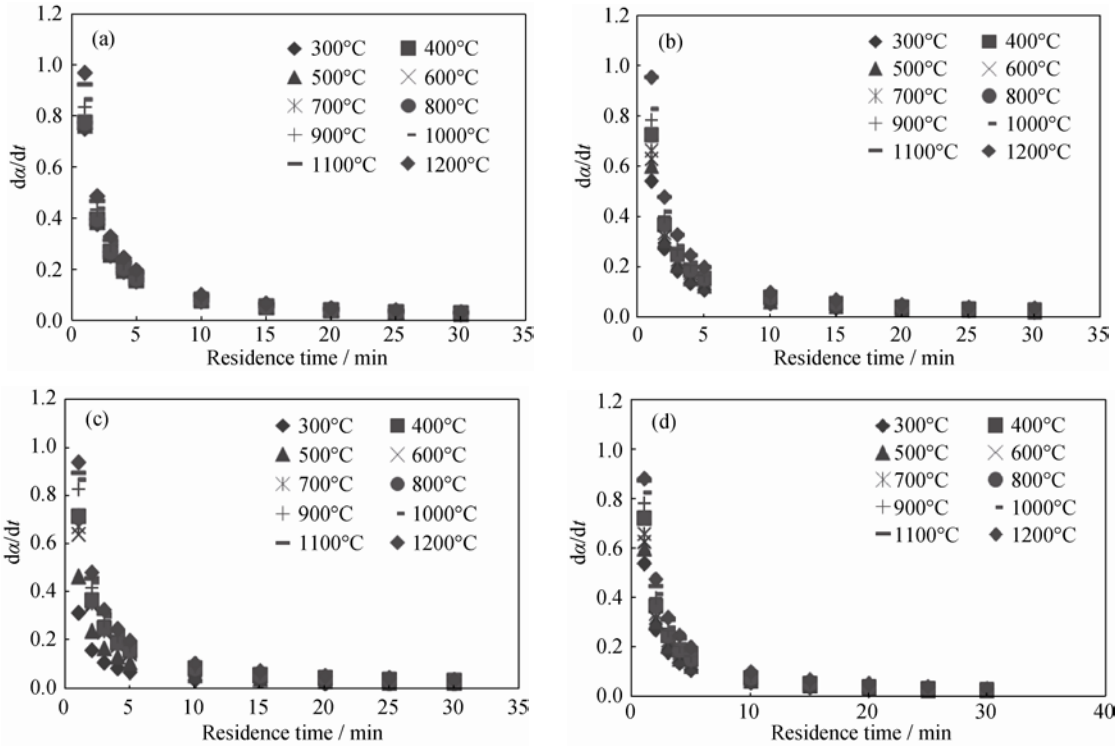

Fig. 7. Rate of thermal decomposition with time for samples A (a), B (b), C (c), and D (d).

respectively. The rate of decomposition is higher at higher temperatures. Subsequently, the rate falls sharply with increasing residence time, which is attributed to starvation of reactant (i.e., LOI). The same trend was observed for all of the samples.

We analyzed most of the isothermal kinetics for solid-state reactions to study the kinetics of the rate of removal of LOI from hydrated iron ore. We modified the raw data to obtain various functional forms of α. The data are plotted against reduced time, $t/t_{0.5}$, to determine the reaction kinetics. Various α-functions for solid-state reduction considered in the present study are presented in Table 4. In Table 4, $D_1(\alpha)$ to $D_4(\alpha)$ represent the cases where the rate was controlled by diffusion, whereas $R_2(\alpha)$ and $R_3(\alpha)$ represent the cases where the rate mechanism followed chemical kinetics. Parameters $A_2(\alpha)$ and $A_3(\alpha)$ represent cases where the reaction was controlled by nucleation and growth. $F_1(\alpha)$ represent the case of first-order kinetics.

Table 4. α-Functions for most commonly used solid-state reaction processes (α represents the fractional reaction, and k and t represent the rate constant and time, respectively).

Rate-controlling process	Kinetic equation
Diffusion, one dimensional	$D_1(\alpha)$: $\alpha^2 = kt$
Diffusion, two dimensional	$D_2(\alpha)$: $(1-\alpha)\ln(1-\alpha) + \alpha = kt$
Diffusion, three dimensional (spherical symmetry)	$D_3(\alpha)$: $[1-(1-\alpha)^{1/3}]^2 = kt$
Diffusion, three dimensional (contracting sphere model)	$D_4(\alpha)$: $1-(2/3)\alpha(1-\alpha)^{2/3} = kt$
Moving phase boundary, two dimensional	$R_2(\alpha)$: $1-(1-\alpha)^{1/2} = kt$
Moving phase boundary, three dimensional	$R_3(\alpha)$: $1-(1-\alpha)^{1/3} = kt$
Random nucleation, two dimensional	$A_2(\alpha)$: $[-\ln(1-\alpha)]^{1/2} = kt$
Random nucleation, three dimensional	$A_3(\alpha)$: $[-\ln(1-\alpha)]^{1/3} = kt$
First order decay law	$F_1(\alpha)$: $-\ln(1-\alpha) = kt$

Fig. 8 depicts a typical reduced-time plot for sample D at 700°C. Here, various best-fit lines through the experimental data represent various α-functions corresponding to various rate mechanisms. The R^2 values are shown against each best-fit line to assess the goodness of fit of the representing α-functions with the experimental data. The kinetics corresponding to α-functions F_1, R_2, and R_3 were found to represent the experimental data closely (with correlation coefficients greater than 99%), indicating that LOI removal from sample D at 700°C is mainly controlled by chemical kinetics. Similarly, the best-fit lines representing various α-functions with R^2 values for other samples at different temperatures are presented in Table 5. For samples A, B, and C (with relatively low LOIs), the α-functions F_1, R_2, and R_3 follow the experimental data for temperatures up to 900°C; at higher temperatures, the A_2 function also appears, setting the stage for a change in reaction mechanism. These results indicate that, at comparatively lower temperatures, chemical kinetics predominates, whereas beyond 900°C, nucleation and growth begin to dominate the reaction mechanism. For the high-LOI sample (sample D), a diffusion process (indicated by *D*-series functions) controls the overall rate at temperatures up to 600°C. Beyond 600°C, the rate mechanism changes to chemical kinetics (F_1, R_2, and R_3); beyond 900°C, nucleation and growth also begin playing roles in the kinetics (coinciding with the appearance of A_2 functions).

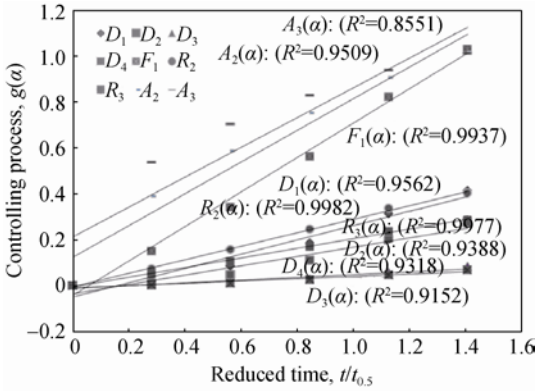

Fig. 8. Best-fit lines for various α-functions for sample D at 700°C.

Table 5 summarizes the kinetic equations that best fit the experimental data with correlation coefficients for various temperatures and samples.

To reinstate the kinetics analysis, we estimated the activation energy values for four different samples; typical Arrhenius plots are shown in Figs. 9(a)–9(d), for samples A, B, C, and D, respectively. The estimated activation energy values for different samples and at different temperature regimes are presented in Table 6.

Table 5. Various α-functions that fit the present experimental data for different samples and temperatures

Temperature / °C	Sample A	Sample B	Sample C	Sample D
300	$F_1(\alpha)$: (R^2 = 0.9853) $R_2(\alpha)$: (R^2 = 0.9982) $R_3(\alpha)$: (R^2 = 0.9958)	$F_1(\alpha)$: (R^2 = 0.9965) $R_2(\alpha)$: (R^2 = 0.9978) $R_3(\alpha)$: (R^2 = 0.9980)	$F_1(\alpha)$: (R^2 = 0.9966) $R_2(\alpha)$: (R^2 = 0.9951) $R_3(\alpha)$: (R^2 = 0.9958)	$D_1(\alpha)$: (R^2 = 0.8987) $D_2(\alpha)$: (R^2 = 0.9020) $D_3(\alpha)$: (R^2 = 0.9052) $D_4(\alpha)$: (R^2 = 0.8977)
400	$F_1(\alpha)$: (R^2 = 0.9841) $R_2(\alpha)$: (R^2 = 0.9978) $R_3(\alpha)$: (R^2 = 0.9952)	$F_1(\alpha)$: (R^2 = 0.9959) $R_2(\alpha)$: (R^2 = 0.9978) $R_3(\alpha)$: (R^2 = 0.9979)	$F_1(\alpha)$: (R^2 = 0.9952) $R_2(\alpha)$: (R^2 = 0.9937) $R_3(\alpha)$: (R^2 = 0.9944)	$D_1(\alpha)$: (R^2 = 0.9436) $D_2(\alpha)$: (R^2 = 0.9384) $D_3(\alpha)$: (R^2 = 0.9322) $D_4(\alpha)$: (R^2 = 0.9368)
500	$F_1(\alpha)$: (R^2 = 0.9854) $R_2(\alpha)$: (R^2 = 0.9982) $R_3(\alpha)$: (R^2 = 0.9960)	$F_1(\alpha)$: (R^2 = 0.9954) $R_2(\alpha)$: (R^2 = 0.9984) $R_3(\alpha)$: (R^2 = 0.9982)	$F_1(\alpha)$: (R^2 = 0.9983) $R_2(\alpha)$: (R^2 = 0.9977) $R_3(\alpha)$: (R^2 = 0.9983)	$D_1(\alpha)$: (R^2 = 0.8924) $D_2(\alpha)$: (R^2 = 0.9112) $D_3(\alpha)$: (R^2 = 0.9309) $D_4(\alpha)$: (R^2 = 0.9184)
600	$F_1(\alpha)$: (R^2 = 0.9858) $R_2(\alpha)$: (R^2 = 0.9989) $R_3(\alpha)$: (R^2 = 0.9967)	$F_1(\alpha)$: (R^2 = 0.9984) $R_2(\alpha)$: (R^2 = 0.9949) $R_3(\alpha)$: (R^2 = 0.9885)	$F_1(\alpha)$: (R^2 = 0.9939) $R_2(\alpha)$: (R^2 = 0.9924) $R_3(\alpha)$: (R^2 = 0.9904)	$D_1(\alpha)$: (R^2 = 0.9745) $D_2(\alpha)$: (R^2 = 0.9762) $D_3(\alpha)$: (R^2 = 0.9750) $D(\alpha)$: (R^2 = 0.9762)
700	$F_1(\alpha)$: (R^2 = 0.9852) $R_2(\alpha)$: (R^2 = 0.9989) $R_3(\alpha)$: (R^2 = 0.9965)	$F_1(\alpha)$: (R^2 = 0.9929) $R_2(\alpha)$: (R^2 = 0.9987) $R_3(\alpha)$: (R^2 = 0.9980)	$F_1(\alpha)$: (R^2 = 0.9904) $R_2(\alpha)$: (R^2 = 0.9987) $R_3(\alpha)$: (R^2 = 0.9979)	$F_1(\alpha)$: (R^2 = 0.9937) $R_2(\alpha)$: (R^2 = 0.9982) $R_3(\alpha)$: (R^2 = 0.9977)
800	$F_1(\alpha)$: (R^2 = 0.9844) $R_2(\alpha)$: (R^2 = 0.9984) $R_3(\alpha)$: (R^2 = 0.9960)	$R_2(\alpha)$: (R^2 = 0.9986) $R_3(\alpha)$: (R^2 = 0.9968) $F_1(\alpha)$: (R^2 = 0.9880)	$F_1(\alpha)$: (R^2 = 0.9897) $R_2(\alpha)$: (R^2 = 0.9984) $R_3(\alpha)$: (R^2 = 0.9971)	$F_1(\alpha)$: (R^2 = 0.9910) $R_2(\alpha)$: (R^2 = 0.9960) $R_3(\alpha)$: (R^2 = 0.9945)
900	$R_2(\alpha)$: (R^2 = 0.9976) $R_3(\alpha)$: (R^2 = 0.9964) $A_2(\alpha)$: (R^2 = 0.9688) $F_1(\alpha)$: (R^2 = 0.9934)	$R_2(\alpha)$: (R^2 = 0.9978) $R_3(\alpha)$: (R^2 = 0.9948) $A_2(\alpha)$: (R^2 = 0.9707) $F_1(\alpha)$: (R^2 = 0.9819)	$R_2(\alpha)$: (R^2 = 0.9973) $R_3(\alpha)$: (R^2 = 0.9931) $F_1(\alpha)$: (R^2 = 0.9752) $A_2(\alpha)$: (R^2 = 0.9775)	$R_2(\alpha)$: (R^2 = 0.9966) $R_3(\alpha)$: (R^2 = 0.9909) $F_1(\alpha)$: (R^2 = 0.9792) $A_2(\alpha)$: (R^2 = 0.9697)
1000	$R_2(\alpha)$: (R^2 = 0.9934) $R_3(\alpha)$: (R^2 = 0.9869) $A_2(\alpha)$: (R^2 = 0.9784)	$R_2(\alpha)$: (R^2 = 0.9970) $R_3(\alpha)$: (R^2 = 0.9923) $A_2(\alpha)$: (R^2 = 0.9775) $F_1(\alpha)$: (R^2 = 0.9736)	$R_2(\alpha)$: (R^2 = 0.9963) $R_3(\alpha)$: (R^2 = 0.9895) $A_2(\alpha)$: (R^2 = 0.9817)	$A_2(\alpha)$: (R^2=0.9824) $R_2(\alpha)$: (R^2=0.9960) $R_3(\alpha)$: (R^2=0.9887)
1100	$R_2(\alpha)$: (R^2 = 0.9927) $R_3(\alpha)$: (R^2 = 0.9847) $A_2(\alpha)$: (R^2 = 0.9816) $F_1(\alpha)$: (R^2 = 0.9605)	$R_2(\alpha)$: (R^2 = 0.9937) $R_3(\alpha)$: (R^2 = 0.9871) $A_2(\alpha)$: (R^2 = 0.9797) $F_1(\alpha)$: (R^2 = 0.9672)	$R_2(\alpha)$: (R^2 = 0.9937) $R_3(\alpha)$: (R^2 = 0.9871) $A_2(\alpha)$: (R^2 = 0.9797)	$R_2(\alpha)$: (R^2=0.9947) $R_3(\alpha)$: (R^2=0.9886) $A_2(\alpha)$: (R^2=0.9772) $F_1(\alpha)$: (R^2=0.9700)
1200	$R_2(\alpha)$: (R^2 = 0.9900) $R_3(\alpha)$: (R^2 = 0.9794) $A_2(\alpha)$: (R^2 = 0.9856)	$R_2(\alpha)$: (R^2 = 0.9900) $R_3(\alpha)$: (R^2 = 0.9806) $A_2(\alpha)$: (R^2 = 0.9872)	$R_2(\alpha)$: (R^2 = 0.9902) $R_3(\alpha)$: (R^2 = 0.9809) $A_2(\alpha)$: (R^2 = 0.9859)	$R_2(\alpha)$: (R^2=0.9947) $R_3(\alpha)$: (R^2=0.9886) $A_2(\alpha)$: (R^2=0.9772) $F_1(\alpha)$: (R^2=0.9700)

In the case of Fig. 9, we note that two separate lines with different slopes best fit the data in two different temperature regimes for the low-LOI samples (A and B) and three separate lines with three different slopes best fit the data for the high-LOI samples (C and D). These results clearly indicate the change in activation energy values and kinetics beyond a certain temperature. In the case of the low-LOI samples, the kinetics is initially slow, as indicated by the small slope and low activation energy, which are attributable to heat-transfer-limited physical moisture removal at temperatures below 700°C. This moisture removal step is followed by a mechanism characterized by a comparatively steep slope and high activation energy value at later stage (beyond 700°C); this later stage is attributed to a shift of the reaction kinetics from heat-transfer control to chemical-kinetics control, which is highly sensitive to temperature. In the case of the high-LOI samples (C and D), the kinetics is initially diffusive (up to 450°C), as indicated by the very small slope, followed by chemical kinetics (steep slope) in the temperature range from 450 to 650°C. At higher temperatures (beyond 650°C), a mechanism characterized by small slope again prevails. The initial small slope is attributed to heat-transfer-limited physical moisture removal, followed by removal of matrix moisture, which is controlled by

chemical kinetics in the intermediate temperature range (450 to 650°C). At high temperatures (beyond 650°C), flattening of the slope is attributed to a process controlled by nucleation and growth of LOI, which is also supported by the reduced plot analysis, where the A_2 function is observed to appear at high temperatures.

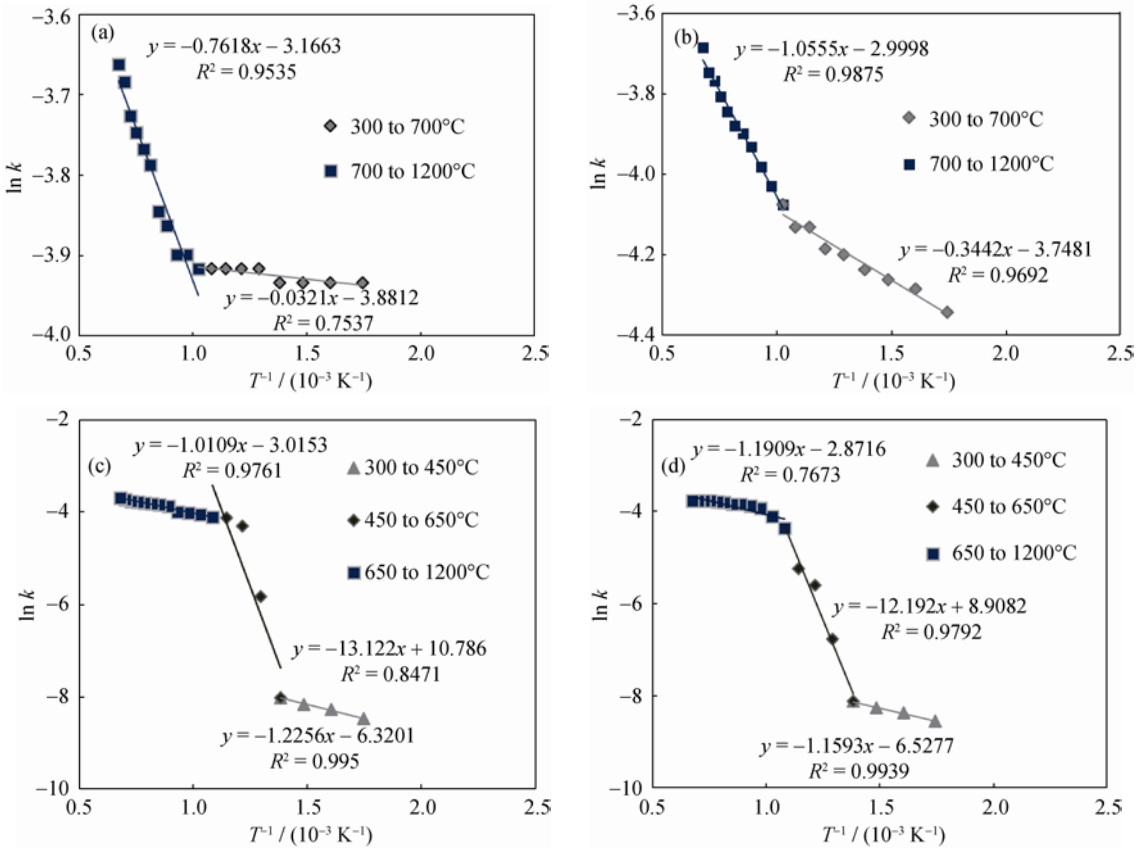

Fig. 9. Arrhenius plots for samples A (a), B (b), C (c), and D (d).

Table 6. Activation energy values for various samples, as estimated for different temperature ranges using Arrhenius plots

Sample	Temperature range / °C	Slope = $-E_a/R$	Activation energy, E_a / (kJ·mol^{-1})
Sample A	300 to 700	–0.0321	0.27
	700 to 1200	–0.7618	6.33
Sample B	300 to 700	–0.3442	2.86
	700 to 1200	–1.0555	8.77
Sample C	300 to 450	–1.2256	10.18
	450 to 650	–13.1220	109.04
	650 to 1200	–1.0109	8.40
Sample D	300 to 450	–1.1593	9.63
	450 to 650	–12.1920	101.32
	650 to 1200	–1.1909	9.90

The activation energy values reported in the literature are for decomposition of synthetic pure goethitic samples or for decomposition of carbonates and hydrates; all of these literature experiments were carried out using low-mass systems under static conditions [17–18]. These previously reported activation energy values were on the order of 100 to 110 kJ/mol. Notably, the activation energies reported here correspond to a high-mass system in a fluidized bed and to natural low-grade hydrated hematite ore. Our values do not represent the intrinsic activation energy; rather, they represent the apparent activation energy, which may also depend on the composition of the ore and on heat and mass transfer. Therefore, a comparison of the present estimated values with the literature values, which mostly represent the intrinsic activation energy in the absence of a complex rate mechanism involving heat, mass transfer, and the effect of impurities on the reaction, is in appropriate. The present study, for the first time, establishes the rate mechanisms for fluidized-bed roasting of hydrated low-grade goethitic hematite ore for LOI removal.

5. Conclusions

(1) The reduction of LOI from hydrated hematite ore in a

laboratory-scale FBR was studied for four different samples with varying LOI contents. The experiments were carried out in the temperature range from 300 to 1200°C and for different residence time ranging from 1 to 30 min. We observed that majority of LOI can be removed in 1 min at temperatures greater than 900°C.

(2) In the FBR, the residence time exerted a minimal effect beyond 5 min; temperature basically dictated the extent of matrix moisture removal, especially in the case of high-LOI samples.

(3) The kinetics of thermal decomposition of hydrated minerals in hematite was studied using plots of various α-functions against reduced time and through estimates of the activation energy. We observed a shift in the kinetics of removal of LOI from hydrated hematite ore beyond a certain temperature. In the case of low-LOI samples, the LOI removal mechanism is controlled by diffusion at a lower temperature and shifts to chemical kinetics at higher temperatures, and the rate becomes less temperature sensitive and follows nucleation-and-growth kinetics.

(4) In the case of high-LOI samples, at temperatures of 450°C or less, the rate followed diffusion kinetics; at temperatures between 450°C and 650°C, it followed chemical kinetics. At higher temperatures, nucleation-and-growth kinetics became dominant.

Acknowledgement

The authors are thankful to the Ministry of Steel, New Delhi for sponsoring the research work undertaken in the present study.

References

[1] S.K. Das, B. Das, R. Saktivel, and B.K. Mishra, Mineralogy, microstructure, and chemical compositions of goethites in some iron ore deposits of Orissa, India, *Miner. Process. Extr. Metall. Rev.*, 31(2010), No. 2, p. 97.

[2] B.K. Mishra, B. Das, S. Prakash, S.K. Das, S. K. Biswal, and P.S.R. Reddy, Issues relating characterization and beneficiation of low grade iron ore, *Steelworld*, November 2007, p. 34.

[3] S.K. Biswal, Utilization of low grade iron ore fines, slimes and tailings by physical beneficiation to minimize the waste generation, *J. Sustainable Planet*, 1(2010), p. 46.

[4] U.C. Chung, I.O. Lee, H.G. Kim, V. Sahajwalla, and W.B. Chung, Degradation characteristics of iron ore fines of a wide size distribution in fluidized-bed reduction, *ISJI Int.*, 38(1998), No. 9, p. 943.

[5] N.S. Sundarmurti and V. Rao, Thermal conductivity and diffusivity of iron ore pellet having low porosity, *ISJI Int.*, 42(2002), No. 7, p. 800.

[6] L.D. Santos and P.R.G. Brandao, Morphological varieties of goethite in iron ore from Minas Gerais, Brazil, *Miner. Eng.*, 16(2003), No. 11, p. 1285.

[7] R.K. Singh, and G.K. Roy, Prediction of minimum bubbling velocity, fluidization index and range of particulate fluidization for gas–solid fluidization in cylindrical and non-cylindrical beds, *Powder Technol.*, 159(2005), No. 3, p. 168.

[8] S. Gialanella, F. Girardi, G. Ischia, I. Lonardelli, M. Mattarelli, and M. Montagna, On the goethite to hematite phase transformation, *J. Therm. Anal. Calorim.*, (102)2010, No. 3, p. 867.

[9] M. Inoue, K. Kitamura, H. Tanino, H. Nakayama, and T. Inui, Alcohothermal treatments of gibbsite: mechanism for the transformation of boehmite, *Clays Clay Miner.*, 37(1989), p. 71. Clays and Clay Minerals

[10] C.H. Bamford and C.F.H. Tipper, eds., *Comprehensive Chemical Kinetics*, Elsevier Scientific Publishing Corporation, Amsterdam, New York, 1980.

[11] I. Halikia, L. Zoumpoulakis, E. Christodoulou, and D. Prattis, Kinetic study of the thermal decomposition of calcium carbonate by isothermal method of analysis, *Eur. J. Miner. Process. Environ. Prot.*, 1(2001), No. 2, p. 1303.

[12] I. Halikia, P. Neou-Syngouna, and D. Kolitsa, Isothermal kinetic analysis of the thermal decomposition of magnesium hydroxide using thermo gravimetric data, *Thermochim. Acta*, 320(1998), No. 1-2, p. 75.

[13] C.J. Goss, The kinetics and reaction mechanism of the goethite to hematite transformation, *Mineral. Mag.*, 51(1987), p. 437.

[14] E. Wolska, Relation between the existence of hydroxyl ions in the anionic substance of hematite and its infrared and X-ray characteristics, *Solid State Ionics*, 28-30(1988), p. 1349.

[15] Ö. Özdemir and D.J. Dunlop, Intermediate magnetite formation during dehydration of goethite, *Earth Planet. Sci. Lett.*, 177(2000), No. 1-2, p. 59.

[16] K. Przepiera and A. Przepiera, Kinetic of thermal transformations of precipitated magnetite and goethite, *J. Therm. Anal. Calorim.*, 65(2001), No. 2, p. 497.

[17] J. Lima-De-Faria, Dehydration of goethite and diaspore, *Z. Kristallogr.*, 119(1963), No. 1-6, p. 176.

[18] P.S.R. Prasad, K.S. Prasad, V.K. Chaitanya, E.V.S.S.K. Babu, B. Sreedhar, and S.R. Murthy, *In situ* FTIR study on the dehydration of natural goethite, *J. Asian Earth Sci.*, 27(2006), No. 4, p. 503